Proceedings of the 2nd International Conference on Fluid Flow, Heat and Mass Transfer
Ottawa, Ontario, Canada, April 30 – May 1, 2015
Paper No. 146

Natural Convection from Horizontal Rectangular Fin Arrays within Perforated Chassis

I-Wen Chou, Shwin-Chung Wong
Department of Power Mechanical Engineering,
National Tsing Hua University,
Hsin-Chu, 300, Taiwan, R. O. C.
scwong@pme.nthu.edu.tw

Abstract **–** In this study, the effects of chassis perforation on natural convection from a horizontal rectangular-fin heat sink have been studied numerically. The results show that when the upper chassis wall is perforated, with a single perforation or multiple dispersed perforations, over the middle region of the heat sink, the venting flow can be smooth and fast, yielding effective cooling of the heat sink. For the optimum perforation layout with an overall opening ration of 0.24, the heat transfer coefficient for the heat sink can be three times as large as that without perforation on the upper chassis wall. If the total length of the perforations is insufficient, the rising heated air is partially blocked and the thermal performance is lowered.

Keywords**:** Natural convection; Fin array; Shrouded fin, Chassis perforation

Nomenclature

A_w	wall area per half channel of the heat sink [m^2]
C	clearance between the top of heat sink and lower surface of chassis [mm]
g	gravitational acceleration [m/s^2]
h	average convection heat transfer coefficient over heat sink, $Q/A_w(T_b-T_\infty)$ [W/m^2K]
H	fin height [mm]
k	thermal conductivity of air [W/mK]
L	half-length of the fin [mm]
L_t	total length of the perforated region in x-direction [mm]
p	pressure [Pa]
Q	convection heat transfer per half channel of the heat sink [W]
S	fin spacing [mm]
t_b	fin base thickness [mm]
t_f	fin thickness [mm]
T	temperature [K]
T_b	fin base temperature [K]
T_0	ambient temperature [K]
u, v, w	velocity in the x, y, z direction, respectively
x, y, z	coordinate directions

Greek Symbols

α	thermal diffusivity
β	coefficient of thermal expansion
η_l	local opening ratio on upper chassis wall
η_o	overall opening ratio on upper chassis wall
η_s	opening ratio on side chassis wall
μ	viscosity
ρ	density
ρ_0	ambient density

1. Introduction

The fan-less thermal solution for electronic devices has drawn considerable attention in recent years for its advantages of low noise, low power consumption, and minimum maintenance. For example, it is used in low-power thin client computers applied in cloud network. In these devices, heat from the CPU is first spread to a finned heat sink and dissipated out through the chassis perforations mainly by natural

convection. One key issue, among others, for optimum thermal design is associated with the layout of chassis perforations. The position, size, and pattern of the perforations can be important to natural convection performance. However, study on natural convection from finned surfaces within a perforated enclosure is rare in the literature. The present work studies the effects of the chassis perforations on the natural convection from a horizontal rectangular-fin heat sink within a perforated chassis.

Harahap and McManus (1967) experimentally studied the natural convection from unshrouded horizontal rectangular fin arrays with different fin lengths (2*L*). For shorter fin arrays, the airflow in the fin channel was able to reach the middle of the fin array venting out due to buoyancy, as opposite to the cases with longer fin arrays. Such a stable flow pattern was called as single chimney flow. For long fins, the plume appeared sliding periodically along the channel direction, as called the sliding-chimney flow. Wong and Huang (2013) performed 3D unsteady numerical analysis to simulate the experiments of Harahap and McManus (1967). Their numerical results verified the observations of Harahap and McManus (1967) that the oscillating sliding-chimney flow tends to appear with increasing fin length (2*L*). The effects of *L*, *H*, and *S* on the average heat transfer coefficient, as well as the dependence of the optimum *S* on *L* and *H*, were also investigated.

Inada et al. (1999) experimentally studied the heat transfer performances of vertical fins in a closed cavity with different material and different numbers. The effects of different height/channel-width ratios were examined. Arquis and Rady (2005) performed 2D numerical simulation and verified the experimental data of Inada et al. (1999). Nada (2007) further extended this subject with different fin spacings, fin heights and fin orientations.

Another configuration available in the literature is concerning a horizontal heat sink shrouded above (Shyu, et al., 2013; Naik et al., 1987). Naik et al. (1987) measured the heat transfer from above-shrouded fin arrays with different fin heights, fin spacings, and clearances at a fixed fin length of 250 mm. Their results reflected that if the clearance is sufficiently large, the heat transfer performance is similar to that of an unshrouded heat sink. Yalcin et al. (2008) conducted three-dimensional simulations for the experiments of Naik et al. (1987).

As can be seen from the literature, studies on natural convection from horizontal heat sinks with a perforated shroud, pertaining to the configuration of electronic devices with a perforated chassis, are unavailable. Consequently, this study aims to explore the effects of shroud perforations on the natural convection from a horizontal heat sink.

2. Theoretical Model

2. 1. Computational Domain

In the numerical analysis for natural convection from a fin array are usually simplified into a single-channel analysis (Arquis and Rady, 2005; Yalcin et al., 2008; Huang et al., 2013; Wong and Huang, 2013). Huang et al. (2014) verified the reliability of such simplification by comparing the results of single-channel analysis with those of multiple-channel analysis. For simplicity, stripe perforations are considered in this study, as shown in Fig. 1(a). In addition, the heat sink is positioned at the middle of the inner bottom surface of the chassis, which has an inner space of 200 mm × 200 mm × 25 mm.

Due to symmetry along the middle plane of the heat sink, half of the single channel is considered, as shown in Fig. 1(c), to save computing resources and time. Heat sink material is aluminum alloy with half-length (*L*) of 50 mm, spacing (*S*) of 8 mm, fin height (*H*) of 20 mm, fin thickness (t_f) of 1.0 mm, and fin base thickness (t_b) of 3 mm, as shown in Fig. 1(b). Stable single-chimney prevails for the present fin length (2*L*) (Harahap and McManus, 1967; Wong and Huang, 2013). The thermal conduction of aluminum alloy is 202.4 W/m K. Chassis material is plastic with a 2 mm thickness and a 100 mm half-length. The clearance (*C*) between the inner surface of chassis and the heat sink top is fixed at 2 mm. The thermal conduction of plastic is 0.15 W/m K. The physical properties of air are treated as temperature dependent.

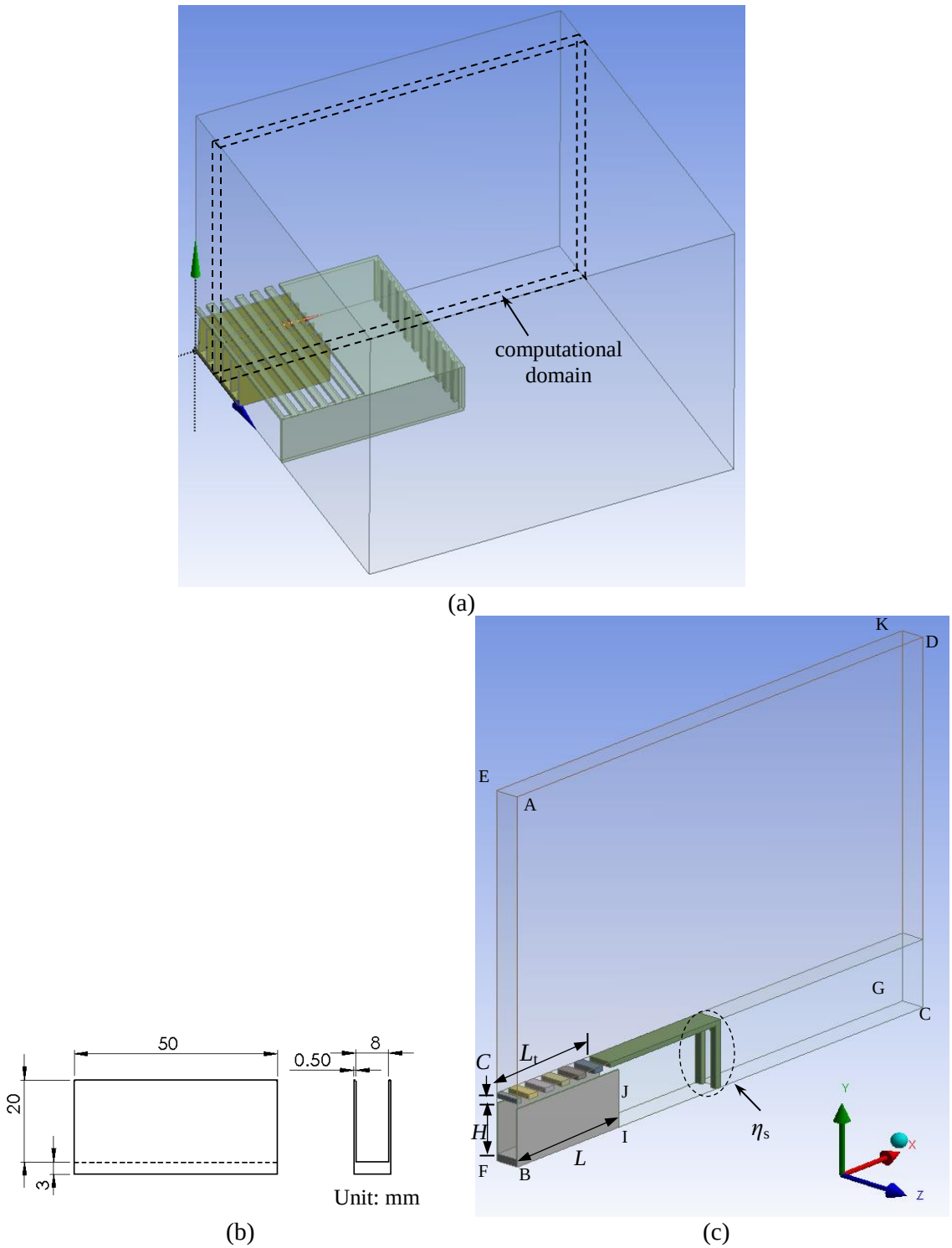

Fig. 1. Computation domain, (a) cut from a quarter of the full chassis; (b) the sizes of a half single channel; (c) half channel with dispersed perforations.

The gravity is 9.81 m/s^2 along negative *y*-direction. Domain size tests show that the differences in the heat transfer coefficient (*h)* are within 1% when the sizes in the *x* and *y* directions are extended from 3*L* and 6*H* to 8*L* and 10*H*, respectively. Finally, the computational dimensions are selected as 4*L*, 7*H*, and

$S+t_f$. Hexahedron grids are adopted. Considering the presence of boundary layers near the solid walls, fine grids are used therein. Grid independence tests indicates that adopting a 0.5 mm grid side within the fin channel and 1 mm side for all other grids outside the boundary layers yields differences within 1% in *h*. The radiation heat losses calculated for selected cases maintain at about 20% of the total heat losses. Therefore, radiation heat loss is ignored in order to focus on the effects of perforations on convection heat transfer.

2. 2. Governing Equations

The following assumptions are made:

1. The air flow field is incompressible and laminar.
2. The fin base temperature (T_b) is fixed at 353K, and the ambient temperature (T_0) is 300 K.
3. Boussinesq approximation is assumed in the buoyancy term, while the fluid density is constant and the other fluid properties temperature-dependent.
4. Radiation heat loss is ignored.

The governing equations can be written as follows:

Continuity equation:

$$\frac{\partial u}{\partial x}+\frac{\partial v}{\partial y}+\frac{\partial w}{\partial z}=0 \tag{1}$$

Momentum equations:

$$u\frac{\partial u}{\partial x}+v\frac{\partial u}{\partial y}+w\frac{\partial u}{\partial z}=-\frac{1}{\rho_0}\frac{\partial p}{\partial x}+\nabla\cdot(\nu\nabla u) \tag{2}$$

$$u\frac{\partial v}{\partial x}+v\frac{\partial v}{\partial y}+w\frac{\partial v}{\partial z}=-\frac{1}{\rho_0}\frac{\partial p}{\partial y}+\nabla\cdot(\nu\nabla v)\ +g\beta(T-T_0) \tag{3}$$

$$u\frac{\partial w}{\partial x}+v\frac{\partial w}{\partial y}+w\frac{\partial w}{\partial z}=-\frac{1}{\rho_0}\frac{\partial p}{\partial z}+\nabla\cdot(\nu\nabla w) \tag{4}$$

Energy equation:

$$u\frac{\partial T}{\partial x}+v\frac{\partial T}{\partial y}+w\frac{\partial T}{\partial z}=\nabla\cdot(\alpha\nabla T) \tag{5}$$

2. 3. Boundary Conditions

Fig. 1(c) shows the boundary conditions of the computational domain. The fin base is held at a constant temperature T_b = 353K (BIJFB surface). Surface ICGJI is treated as the adiabatic because only convection from the heat sink is considered. Symmetric boundary conditions are applied at surfaces ABCDA, ABFEA, and EFGKE. Surfaces CDKGC and ADKEA are open boundaries. Non-slip boundary condition is specified at the fluid-solid interfaces.

3. Numerical Method

The computational domain is meshed via commercial software ANSYS 15.0, and the velocity and temperature distributions are calculated by FLUENT. Second-order upwind scheme is applied for momentum and energy equations. The SIMPLE algorithm (Partankar, 1980) is utilized for pressure correction. Steady-state simulation is performed in all the cases. The residuals for the continuity and momentum equations are under 1×10^{-6}, while those for the energy equation are under 1×10^{-10}.

4. Results and Discussion

In this study, the temperature at the heat sink bottom is fixed at 353 K. Also fixed are the heat sink dimensions and the clearance between heat sink top and the chassis wall of 2 mm. The effects of different perforation lengths or patterns are quantified by the convection heat transfer coefficient (h).

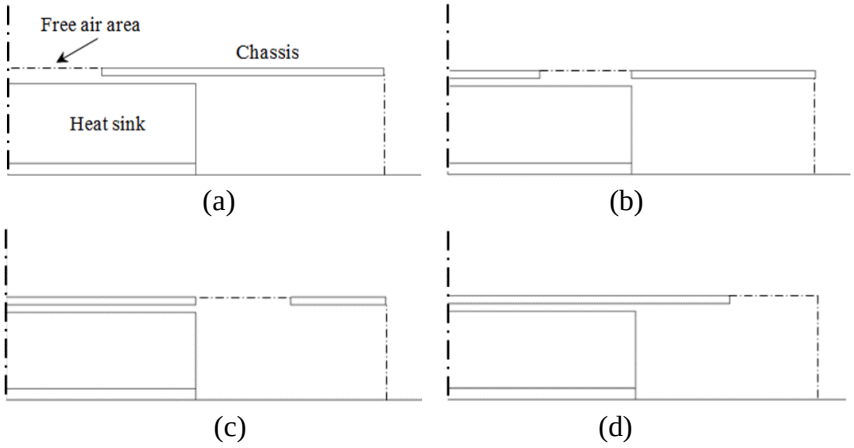

Fig. 2. Schematic diagram of a perforation in different positions on the chassis: (a) Case II; (b) Case III; (c) Case IV; (d) Case V.

4. 1. Cases with Single Perforation

The present study begins with the simplest conditions with single perforation to explore the key factors to the heat transfer performance. All the cases in this section are associated with an opening ratio of the side chassis wall (η_s) of 1.0 (cf. Fig. 1c where η_s = 0.44). The effects of the position and length of the single perforation are discussed as follows.

4. 1. 1. Effects of Perforation Position

In order to investigate the effect of perforation position related to the heat sink, a reference configuration without perforation, designated as Case I, is examined first. Then, four different cases with different perforation positions but an identical perforation length are compared. In Case II, a 25 mm-long perforation is positioned over the middle region of the heat sink. In Case III , IV and V, respectively, the perforation shifts toward the side end of the chassis by a 25 mm distance consecutively, as shown in Fig. 2. Figs. 3 and 4 show the flow and temperature fields of Case I and II, respectively. For Case I, the rising heated air is blocked by the upper wall and forced to exit via the same side, with the heated air flowing against the entering flow, as shown in Fig. 3. Due to the viscous effect of counter-flow, the cool entering air fails to approach the middle region of the heat sink, leaving a wide high-temperature middle region. In contrast, the rising heated air in Case II vents smoothly through the perforation over the middle region of the heat sink and develops a single-chimney flow pattern with smooth streamlines, as shown in Fig. 4. The faster venting air flow is able to reach the middle of heat sink and makes efficient cooling. As the chassis is closed over the middle region of the heat sink asin Case III and Case IV, the air flow has to make a sharp U-turn in front of the middle region of the heat sink. Thus, the convection heat transfer coefficients in Case III and IV are reduced. Because of the farthest position of perforation in Case V, the flow pattern of Case V is similar to that of Case I. Generally speaking, the most favorable condition is when the perforation is located over the middle region of the heat sink. Such a position of perforation leads to smooth and fast venting flow.

4. 1. 2. Effects of Perforation Length

In this section, we further consider different lengths (from 10 mm to 45 mm) of the single perforation located over the middle region of the heat sink. (Note: The perforation length in this work refers to that in

the *x*-direction.) The flow and temperature fields for the cases with 10 mm perforation are shown in Fig. 5, with the case of 25 mm perforation shown in Fig. 4. With the perforation as small as 10 mm, the exiting flow is partially blocked by the upper shroud. The flow resistance is higher than for the case with a larger perforation, as evidenced by the lower air flow rate. For example, the air flow rate passing through the fin channel for a 35 mm perforation is around 1.45 times of that for a 10 mm perforation. The convection heat transfer coefficients for different perforation lengths are compared in Fig. 6. The heat transfer coefficient without perforation on the upper chassis wall is about a third of that for a 25 mm long perforation. When the perforation is longer than 35 mm, a small portion of the cool air is entrained from the space above the chassis through the perforation. This phenomenon causes very slight negative effect, as will be discussed in Section 4.2.

4. 2. Cases with Dispersed Perforations

In real applications, multiple dispersed perforations with limited length are adopted, due to the concerns of dust, mechanical strength, and outlook, etc. Also, the side walls of the chassis are partially opened. In this section, the opening ratio on the side chassis wall (η_s) is selected as 0.44. As to the perforations on the upper chassis wall, the total perforation length is fixed at 24 mm, i.e., the overall opening ratio (η_o) is fixed at 0.24. For the cases with dispersed perforations, six 4 mm-long perforations are separated by different rib lengths of 0, 1, 2, and 4 mm, respectively. These arrangements form different perforation layout covering the middle of the chassis with the total length of perforated region (L_t) ranging from 24 mm to 46 mm. In the latter three layouts, the local opening ratio on the upper wall (η_l) is 0.8, 0.66, and 0.5, respectively.

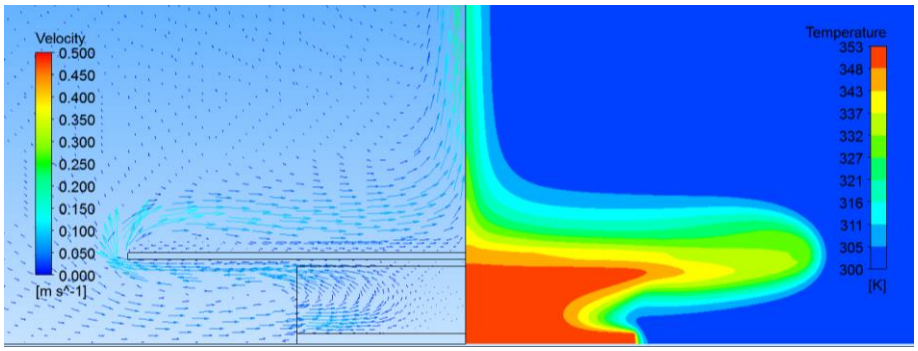

Fig. 3. Velocity and temperature fields for Case I.

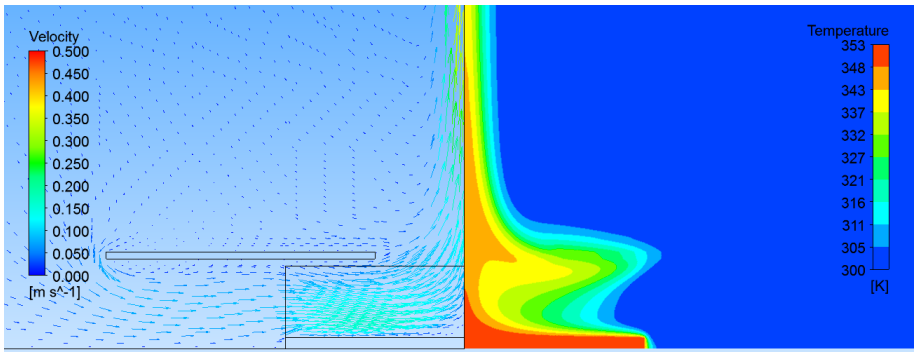

Fig. 4. Velocity and temperature fields for Case II.

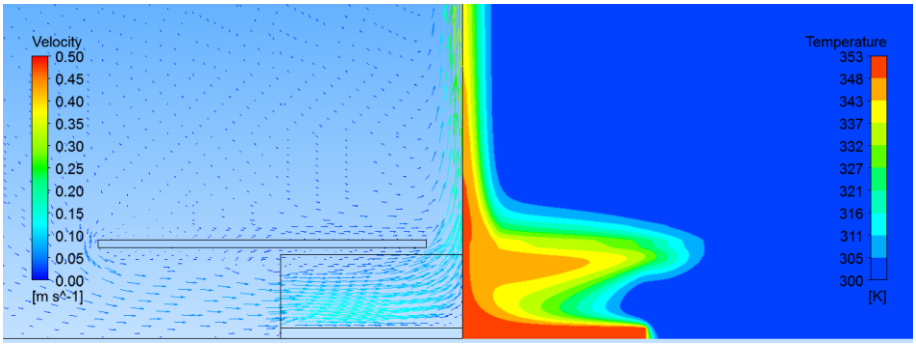

Fig. 5. Velocity and temperature fields for a single perforation with a length of 10mm over the middle of heat sink.

The flow patterns are essentially similar for these four perforation layouts, as that shown in Fig. 4, since the perforated region covers the middle part of the heat sink. The calculated heat transfer coefficients for the above layouts are shown in Fig. 7. The highest *h* appears for perforations separated by 1 mm ribs. For this case, the local opening ratio η_l on the upper wall is 0.8 and the total length of the perforated region is 29.5 mm. The presence of fine ribs shorter than 2 mm exhibits an insignificant effect on the convective flow. However, when the rib is 4 mm long, the heat transfer performance is slightly deteriorated. In this case, the ribs partially block the rising air flow to increase flow resistance. In addition, when there are perforations over the region near the fin end, a small portion of cool air is entrained into the chassis from above through the perforations, rather than through the side opening. When the cool air is entrained from the fin side, it would flow through the fin channel with efficient cooling of the heat sink. However, the cool air entrained from above is less efficient in cooling because it would only flow by the upper part of the fins.

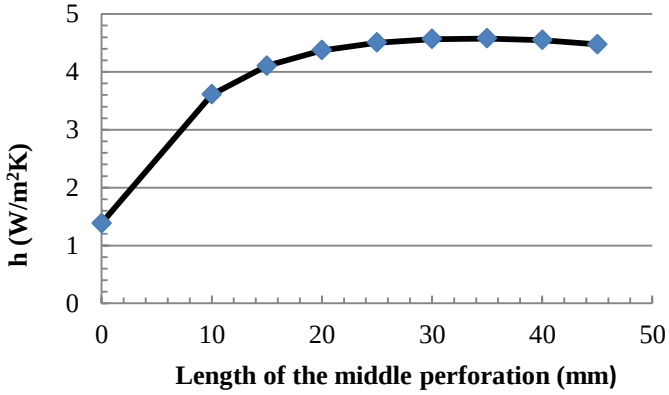

Fig. 6. Convection heat transfer coefficients for different lengths of the middle perforation.

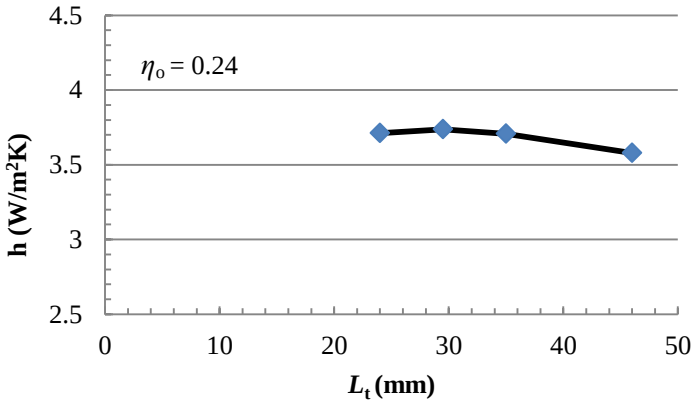

Fig. 7. Convection heat transfer coefficients for different lengths of the perforated region (L_t).

5. Conclusions

In this study, the effects of chassis perforation on natural convection from a horizontal rectangular-fin heat sink have been studied numerically. The following conclusions are reached:

1. When the perforations on the upper chassis wall are laid over the middle region of the heat sink, the venting flow can be smooth and fast to result in effective cooling. For example, such a single perforation with a 25 mm length results in a heat transfer coefficient three times as large as that without perforation on the upper chassis wall.
2. Similar thermal performance is found for a single perforation with a length of 25−45 mm over the middle of the heat sink. But when the single perforation is as short as 10 mm, the rising heated air is partially blocked to exhibit lower thermal performance.
3. If multiple dispersed perforations are made over the middle region of the heat sink, the flow patterns are essentially similar to that of a single perforation with the same total perforation length. The presence of fine ribs between the perforations exhibits an insignificant effect on the convective flow. But for long ribs, which yield smaller local opening ratios and larger total lengths of the perforated region for the same overall opening ratio, the thermal performance is slightly deteriorated.

References

Arquis E., Rady M. (2005). Study of Natural Convection Heat Transfer in a Finned Horizontal Fluid Layer, *Int. J. Therm. Sci.*, 44, 43–52.

Harahap F., McManus H. N. (1967). Natural Convection Heat Transfer From Horizontal Rectangular fin Arrays, *ASME J. Heat Transfer*, 89, 32-38.

Huang G.-J., Wong S.-C. (2012). Dynamic Characteristics of Natural Convection from Horizontal Rectangular fin Arrays, *Appl. Therm. Eng.*, 42, 81-89.

Huang G.-J., Wong S.-C., Lin C.-P. (2014). Enhancement of Natural Convection Heat Transfer from Horizontal Rectangular Fin Arrays with Perforations in Fin Base, *Int. J. Therm. Sci.*, 84, 164-174.

Inada S., Taguchi T., Yang W.J. (1999). Effects of Vertical Fins on Local Heat Transfer Performance in a Horizontal Fluid Layer, *Int. J. Heat Mass Transfer*, 42, 2897–2903.

Nada S. A. (2007). Natural Convection Heat Transfer in Horizontal and Vertical Closed Narrow Enclosures with Heated Rectangular Finned Base Plate, *Int. J. Heat Mass Transfer*, 50, 667–679.

Naik S., Probert S.D., Wood C.I. (1987). Natural-Convection Characteristics of a Horizontally-Based Vertical Rectangular Fin-Array In The Presence of a Shroud, *Appl. Energy*, 28, 295-319.

Patankar S.V. (1980). "Numerical Heat Transfer and Fluid Flow," Hemisphere Publishing.

Shyu J.-C., Hsu K.-W., Yang K.-S., Wang C.-C. (2013). Orientation Effect on Heat Transfer of A Shrouded LED Backlight Panel with A Plate-Fin Array, *Int. Comm. Heat Mass Transfer*, 42, 51–54.

Wong S.-C., Huang G.-J. (2013). Parametric Study on the Dynamic Behavior of Natural Convection from Horizontal Rectangular fin Arrays, *Int. J. Heat Mass Transfer*, 60, 334-342.

Yalcin H. G., Baskaya S., Sivrioglu M. (2008). Numerical Analysis of Natural Convection Heat Transfer from Rectangular Shrouded Fin Arrays on a Horizontal Surface, *Int. Comm. Heat Mass Transfer*, 35, 299–311.